Mineralogy, geochemistry and petrography of methane-derived authigenic carbonates from Enza River, Northern Apennines (Italy)

Mineralogy, geochemistry and petrography of methane-derived authigenic carbonates from Enza River, Northern Apennines (Italy)

I. Viola [a,*], D. Oppo [a], F. Franchi [b,c], R. Capozzi [a], E. Dinelli [a], B. Liverani [a], M. Taviani [b]

[a] Department of Biological, Geological and Environmental Sciences, University of Bologna, Via Zamboni 67, 40126 Bologna, Italy
[b] Institute of Marine Sciences (ISMAR)-CNR, Via Gobetti 101, 40129 Bologna, Italy
[c] Department of Earth and Environmental Sciences, BIUST, Private Bag 16, Palapye, Botswana

ARTICLE INFO

Keywords:
Carbonate chimneys
Hydrocarbon migration
Anaerobic methane oxidation
Apennine chain

ABSTRACT

A remarkable exposure of carbonate pipe like and slab concretions occurs along the Enza riverbanks on the Northern Apennines foothills (Italy). Based upon geochemical and field evidences, their genesis has been attributed to microbial governed carbonate precipitation from hydrocarbon enriched fluids. The pipe like concretions are thus interpreted as former conduits (chimneys) marking sites of methane ascent onto the seafloor. The resulting Enza River chimney field is arranged in a palisade fashion, a rare example of such. Mineralogical and petrographic analyses of some chimneys and slabs document that the dominant cement is dolomite. Although the chimneys show a rather homogeneous texture, a clear zonation is observed in the relative distribution of major and minor elements in their internal and external parts. The occurrence of sulphide minerals in the stratigraphically upper samples indicates possible renewal of fluids leakage after a major erosive event.

1. Introduction

The formation of authigenic carbonates linked to hydrocarbon enriched fluids seepage onto the seafloor is a well known phenomenon. It is documented in modern and ancient marine sedimentary basins worldwide particularly, but not exclusively, in compressive tectonic regimes at convergent margins (e.g., Taviani, 2001; Pinheiro et al., 2003; Nyman et al., 2010; Capozzi et al., 2012). Microbially mediated anaerobic oxidation of methane (AOM) and sulphate reduction (SR) increase the pore water alkalinity, favouring the pre cipitation of methane derived authigenic carbonates (MDAC) (e.g. Boetius et al., 2000; Peckmann and Thiel, 2004; Teichert et al., 2005). Their various morphologies include slabs and crusts, cylindrical and pipe like conduits, and irregularly shaped bodies (e.g. Taviani, 2001; Clari et al., 2004; Lein, 2004; Magalhaes et al., 2012). Pipe like con duits are the less reported in literature and their formation mecha nisms are still under debate (e.g. Nyman et al., 2010; Magalhaes et al., 2012; Oppo et al., in this issue).

Increasing attention is presently devoted to understanding pipe-like concretions characteristics and formative processes (e.g., Orpin, 1997; Díaz del Rio et al., 2001, 2003; Somoza et al., 2003; De Boever et al., 2006a,b; Nyman et al., 2010; Magalhaes et al., 2012; Oppo et al., in this issue; Angeletti et al., in this issue). The seep carbonates show characteristic mineralogy and geochemistry, as the authigenic carbonate minerals, such as dolomite, calcite and aragonite, which compose the MDAC concretions, are usually over than 50% bulk weight. Their relative amounts depend on the formation environment and on the fluids involved in the precipitation (e.g. Peckmann and Thiel, 2004; Magalhaes et al., 2012; Vanneste et al., 2012). Being considered as indicators of hydrocarbon seepages, authigenic carbonates testify the present day or past occurrence of petroleum generation systems (Capozzi et al., 2012; Oppo et al., 2013; Unterseh, 2013).

This study provides first detailed mineralogical, geochemical and petrographic information on hydrocarbon imprinted carbonates, from the Enza River succession (Capozzi et al., 2013; Gunderson et al., 2014; Oppo et al., in this issue). In addition, we also provide some compositional data on the host marine sediments for a better characterization of the genetic environments of carbonates. At this site, the formation of methane derived authigenic carbonates is strictly connected with the geologic evolution of the basin (see Oppo et al., in this issue).

2. Geological setting

Intense flooding events over the last few years resulted in a pronounced fluvial incision of the Enza riverbanks in the Northern Apennines foothills (Fig. 1).

* Corresponding author.
E *mail address:* irene.viola3@unibo.it (I. Viola).

Such erosive processes resulted in the exposure downstream the city of San Polo d'Enza of a marine succession punctuated by a number of slab and pipe like carbonate concretions (Fig. 2).

The foothills deformation in the Enza River area started in the Late Miocene and continued until the Pleistocene, resulting in the formation of the Quattro Castella anticline (Boccaletti et al., 2010; Ponza et al., 2010; Gunderson et al., 2014). The Enza River succession belongs to the forelimb of the Quattro Castella anticline and represents a full transition, from muddy shelfal deposits (Argille Azzurre Fm.) to the transitional coastal system (Sabbie Gialle Fm.) (Gunderson et al., 2014, and references therein). The synsedimentary tilting of the anticline led to the variation of strata dip along the 65 m thick studied succession, which progressively changes from 55° at the base to 42° at the top. A corallinaceous rhodolith rich bed, which dips 35°, represents the top of the studied section and identifies an angular unconformity (Gunderson et al., 2014) that marks an erosional discontinuity. The recovering of deposition started with the colonization by benthic epifauna (Oppo et al., in this issue).

The carbonate concretions are enclosed in the Lower Pleistocene Argille Azzurre Fm., which is composed of blue grey silty clays deposited in external continental shelf environment. The carbonate pipe like concretions, in this paper defined as chimneys, and slabs occur between 30 and 65 m of the Enza section (Oppo et al., in this issue). The chimneys have often sub vertical orientation with respect to horizontal and are arranged in a sort of pipe palisade, a rare occurrence seldom seen in outcrop (e.g. De Boever et al., 2006a; Cau et al., in this issue) and submerged situations (e.g. Taviani, 2014) whilst slabs conform to stratification. Morphologies and dimensions vary: pipe like and cylindrical chimneys range from few cm to almost 2 m high, with up to 40 cm in diameter; slabs are few cm to 30 cm thick and up to several metres long (Fig. 2) (see also Capozzi et al., 2013; Gunderson et al., 2014; Oppo et al., in this issue).

3. Materials and methods

Fieldwork was conducted in May 2010 and May 2013 to sample chimneys, slabs and host sediment for their mineralogical, geochemical and petrographical comparative characterization. 31 samples of Argille Azzurre Fm. have been recovered and analysed, together with 4 samples of carbonate concretions: two chimneys (En5 and En10) and two carbonate bodies, one tabular slab (Cr2) and a concretion within the rhodolith rich layer (Cr3) (Fig. 3).

The carbonate concretions have been divided in 29 sub samples to be analysed (Fig. 4).

The En5 chimney does not have an open central vent and is 63 cm long and 20 cm in diameter (Fig. 4a). To investigate eventual geochemical variations along the chimney, it has been cut in 8 sections from the bottom (1) to the top (8). Each section, excluding 1 and 8, has been longitudinally divided in 3 subsamples: internal part (A), central part (B) and external part (C). The En10 chimney is

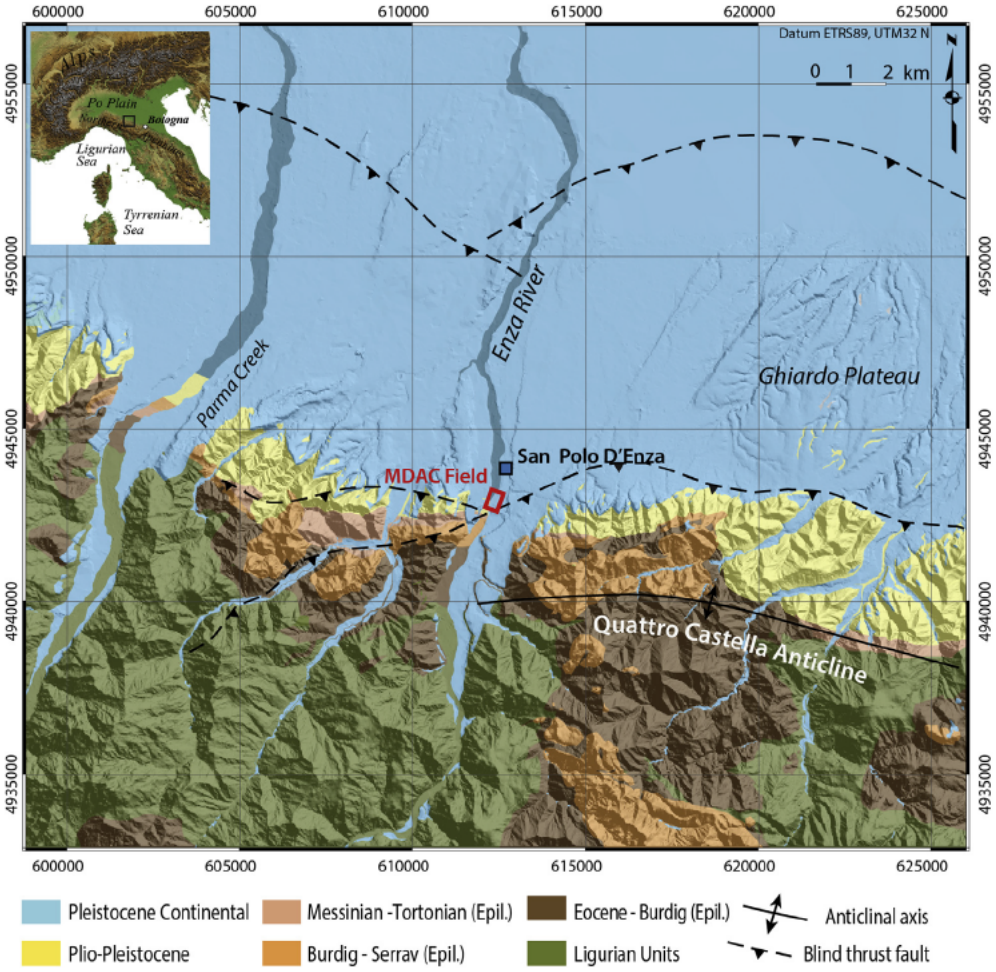

Figure 1. Geological map of the investigated area of the Northern Apennines. The Enza carbonate field (red square) is located along the Enza River near the town of San Polo d'Enza (modified from Oppo et al., in this issue). (For interpretation of the references to colour in this figure legend, the reader is referred to the web version of this article.)

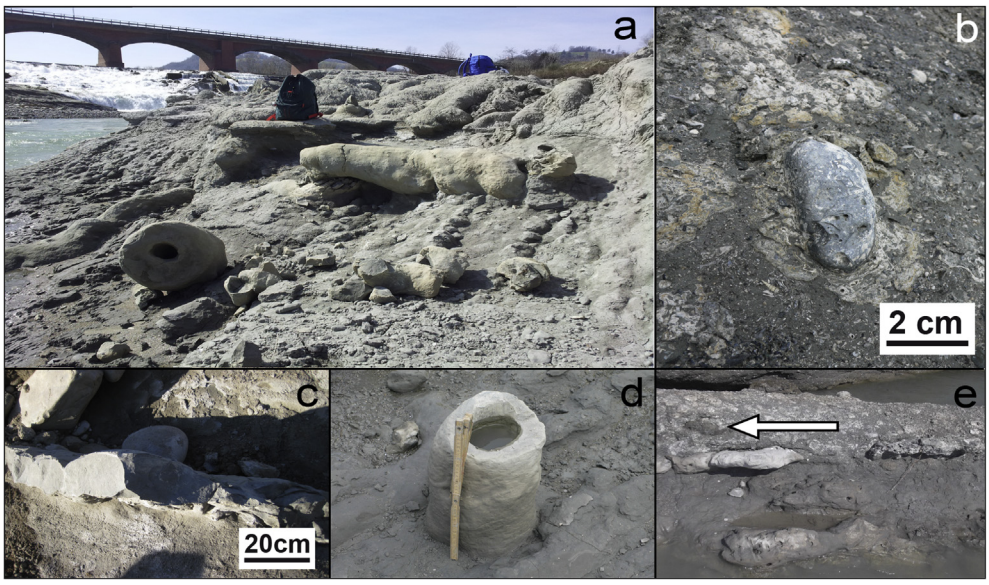

Figure 2. Example of the carbonate concretions occurring along the Enza riverbanks. a) Various concretions have been exposed by the erosion. The observed chimneys reached up to 2 m in length. b) Detail of the rhodolith-rich layer. A fine-grained cemented matrix contains numerous rhodolites and biogenic structures. A dark-grey carbonate pebble is encrusted by red algae. c) Outcropping slab. d) Pipe-like chimney with sub vertical orientation respect to the horizontal. e) The rhodolith-rich bed directly overlies a carbonate slab. Arrow points to dark-grey carbonate enclosed in the bed.

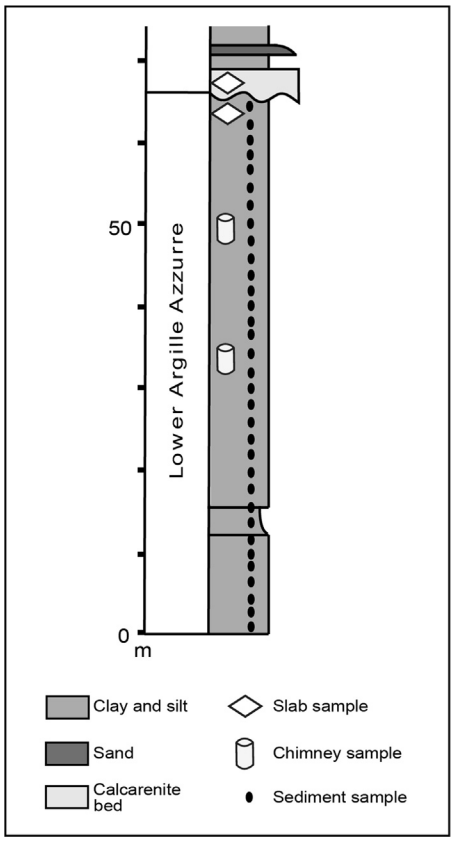

Figure 3. Simplified stratigraphic column of the studied succession along the Enza River. The rhodolith-rich layer marks an erosional unconformity, separating the interval hosting the concretions from the underlying Lower Pleistocene succession. The position of samples discussed in text is marked. Sediments are sampled from 4 to 64 m bottom top; chimney En5 is the lower one, En10 the upper one; slab Cr2 is the one just below the corallinaceus bed, while Cr3 is the one collected inside the corallinaceus bed.

170 cm long and 20 cm in diameter; only the top and the bottom have been analysed (Fig. 4 b and c, respectively). The top subsample has been divided in external (B) and internal (A) portions.

The Cr3 sample is a concretion within the rhodolith rich layer; it shows a dark colour and is well cemented. A dark grey area (Cr3A, Fig. 4d) was analysed and compared with the light grey matrix (Cr3B, Fig. 4e). The Cr2 slab pertained to the carbonate concretions stratigraphically below the rhodolith rich layer; it shows a grey colour with a light grey area (Cr2b in Fig. 4f).

The samples have been powdered, homogenized in agate mortar and analysed for mineralogy by X ray diffractometry (XRD) using a Philips PW 1130 (Cu Kα radiation Ni filtered) in the XRD Laboratory of BiGeA department, Bologna University. Powders were pressed into alumina holders in order to avoid preferential orientation of sheet silicates. Estimates of the relative minerals abundance were determined using MacDiff software packages and carbonate min eral compositional limits defined according to Goldsmith and Graf (1958) and Lumsden (1979).

Nitrogen and Total Organic Carbon (TOC) have been analysed with CHNS pre treating 10 mg of powdered sample in 40 μl of HCl 1.5 N for 2 h in the oven, this procedure have been repeated two times to eliminate all the inorganic carbon traces. The resulting compounds have been analysed to estimate TOC and Nitrogen by CHNS Analizer Flash 2000 Thermo Scientific Gas Chromatographer in Pedology Laboratory, BiGeA department, Ravenna, Bologna University. This analysis was performed only on En5 samples and hosting sediments because the higher number of samples from En5 gives a better representation of the carbonates bodies in all its parts (internal, central and external) and were more accurate for a comparison with the hosting sediments samples.

Major and trace elements have been determined by X ray fluorescence (XRF) spectrometry on pressed powered pellets using a Philips PW 1480 automated spectrometer following the methods of Franzini et al. (1972, 1975), Leoni and Saitta (1976) and Leoni et al.(1982) for matrix corrections in XRF Laboratory, BiGeA department, Bologna University. The estimated precision and accuracy for trace element determinations are more than 5% except for the elements at 10 ppm and lower (10–15%); the detection limit for most of the trace elements is 3 ppm (Leoni and Saitta, 1976).

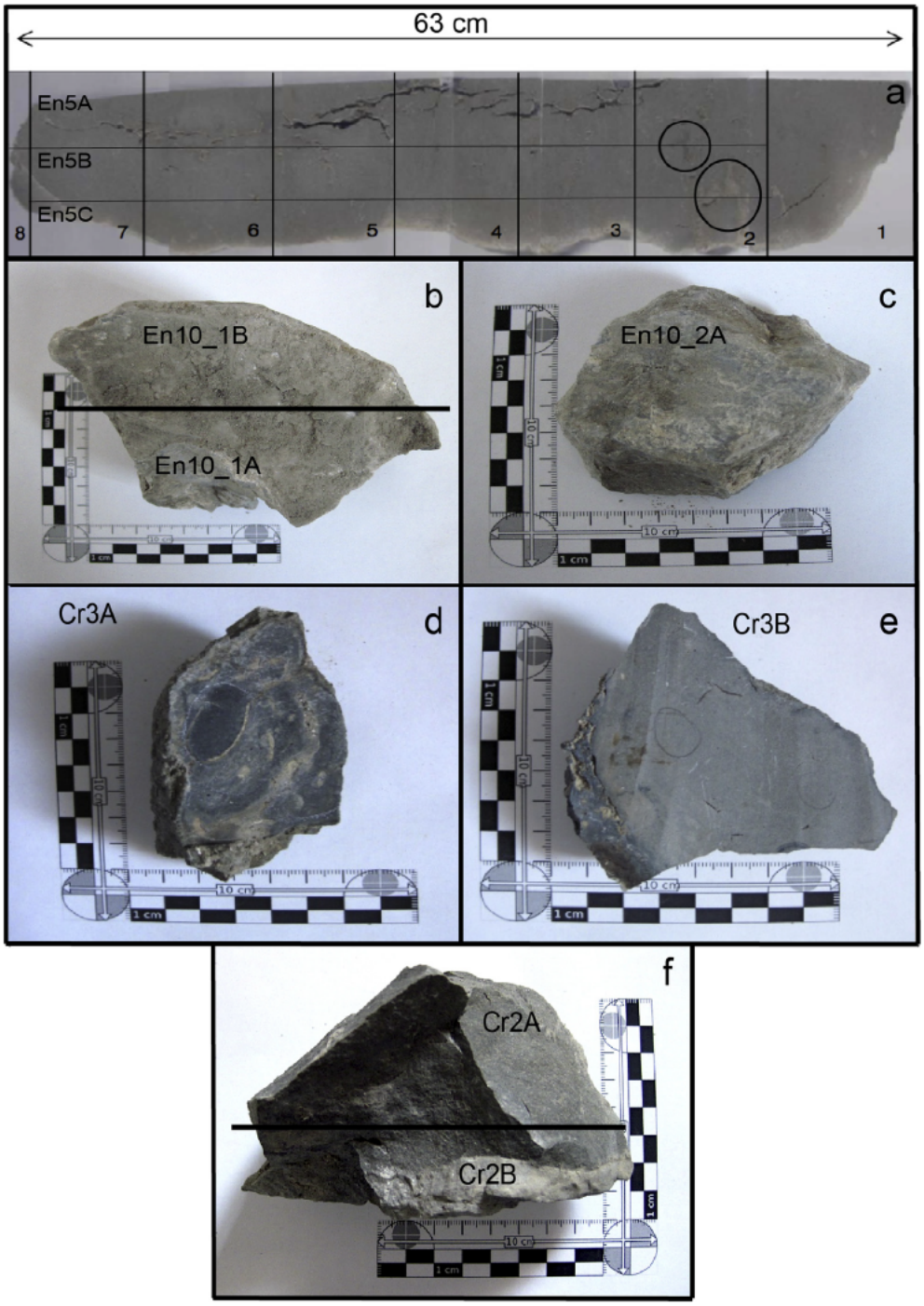

Figure 4. Carbonate samples analysed in this study. a) The En5 chimney that has been divided in 8 sections from bottom to top. Horizontal lines separate the internal (En5A), central (En5B) and external (En5C) subsamples. b) The top of En10 chimney has been divided in external (En10_1B) and internal (En10_1A) portions. c) Bottom of the En10 chimney. d) Cr3A concretion. The dark-grey colour, mainly due to the high sulphide minerals content, can be observed. e) Grey portion of the Cr3 concretion. Along the left edge of the sample can be observed a dark-grey thrombolytic layering. f) The Cr2 slab has been divided in two samples to differentiate the darker part of the concretion (Cr2A) from the lighter-colour of the external area (Cr2B). (For interpretation of the references to colour in this figure legend, the reader is referred to the web version of this article.)

The petrographic and microfacies based analyses were performed on. 80 uncovered thin sections (45 × 60 mm^2 surface area, 30 μm thickness) at the ISMAR CNR, U.O.S. Bologna. Cathodoluminescence petrography was conducted using a CL 8200 MK3 optical equipment (operating conditions: 20 kV beam voltage and 200 μÅ beam current) at the University of Padua. Morphological description and chemical elemental composition of microscopic features were obtained by using a Philips 515 scanning electron microscope (SEM) equipped with an electron back scattering system and EDX (EDAX DX 4) at the SEM Laboratory, BiGeA department University of Bologna. SEM EDX investigations (SEM operating conditions: 15 and 25 kV accelerating voltage) were performed on freshly broken samples (Au coated) and thin sections (C coated).

Carbon and oxygen isotopic analyses have been performed on carbonate samples from Enza River in this study at CNR Institute

Table 1
Mineral abundances in the sediment. Samples position starts from the base of the Enza section.

Samples	Position	Quartz	Chlorite	Muscovite	Calcite	Dolomite	Feldspars	Pladgioclase	Clay minerals	Others
	(m)	(%)	(%)	(%)	(%)	(%)	(%)	(%)	(%)	(%)
4	1.2	20	6	9	21	2	15	10	15	2
12	4.4	27	7	9	18	0	13	6	19	1
17	6.4	23	9	8	19	0	11	10	17	3
22	8.4	16	6	6	28	2	7	11	23	1
27	10.4	11	5	8	31	0	6	14	23	2
32	12.4	24	8	10	19	0	9	15	11	4
37	14.4	15	7	8	25	0	8	5	30	2
42	16.4	21	9	10	20	0	11	6	20	3
47	18.4	18	7	7	22	2	13	11	16	4
52	20.4	17	5	6	28	2	8	9	23	2
57	22.4	24	8	8	17	0	17	4	19	3
62	24.4	16	5	7	29	0	8	6	25	4
67	26.4	26	6	9	19	0	12	11	15	2
72	28.4	17	7	6	26	1	9	13	19	2
77	30.4	23	6	7	21	3	12	10	15	3
82	32.4	18	7	7	22	3	13	8	16	6
88	34.8	25	7	10	14	0	20	12	11	1
92	36.4	24	9	11	15	4	9	8	17	3
97	38.4	21	6	8	15	2	24	7	15	2
102	40.4	13	10	7	23	2	9	10	24	2
107	42.4	21	8	8	20	3	9	9	19	3
113	44.8	12	5	5	31	2	8	14	21	2
117	46.4	25	7	10	17	2	13	12	10	4
122	48.4	14	7	7	25	1	10	4	29	3
127	50.4	25	7	7	20	2	12	9	17	1
132	52.4	13	11	6	23	2	10	12	20	3
137	54.4	20	8	9	21	0	12	10	19	1
142	56.4	25	5	8	17	2	17	8	16	2
147	58.4	32	10	9	13	0	14	6	12	4
152	60.4	16	4	4	30	1	9	14	19	3
157	62.4	24	8	7	18	2	17	7	15	2
162	64.4	21	6	9	20	2	12	7	21	2

Table 2
Major oxides in the sediment. Samples position starts from the base of the Enza section.

Sample	Position	SiO_2	TiO_2	Al_2O_3	Fe_2O_3	MnO	MgO	CaO	Na_2O	K_2O	P_2O_5	LOI	Mg/Ca	Sr/Ca
	(m)	(wt %)	(wt %)	(wt %)	(wt %)	(wt %)	(wt %)	(wt %)	(wt %)	(wt %)	(wt %)	(wt %)		
4	1.20	44.70	0.60	12.25	5.20	0.12	3.31	15.28	0.98	2.11	0.11	15.36	0.1828	0.0041
12	4.40	45.93	0.58	12.67	4.83	0.12	3.41	14.42	1.04	2.16	0.07	14.78	0.1996	0.0042
17	6.40	45.29	0.58	12.25	4.90	0.12	3.39	15.50	1.07	2.12	0.06	14.70	0.1846	0.0043
22	8.40	40.64	0.56	11.88	4.63	0.11	2.94	17.90	0.98	1.96	0.05	18.34	0.1386	0.0041
27	10.40	40.55	0.57	12.34	4.81	0.11	2.77	16.72	0.93	2.15	0.08	18.97	0.1398	0.0048
32	12.40	45.94	0.58	12.84	5.02	0.12	3.31	14.06	1.12	2.13	0.07	14.81	0.1987	0.0046
37	14.40	45.99	0.56	12.45	4.57	0.12	3.17	15.00	1.05	2.07	0.07	14.95	0.1783	0.0049
42	16.40	46.12	0.57	12.60	4.64	0.12	3.35	14.16	0.95	2.11	0.07	15.30	0.1996	0.0037
47	18.40	46.57	0.58	12.80	4.59	0.11	3.28	13.95	0.97	2.14	0.07	14.93	0.1984	0.0044
52	20.40	45.54	0.58	12.92	4.76	0.11	3.36	14.29	1.00	2.15	0.07	15.22	0.1984	0.0036
57	22.40	45.88	0.58	12.85	4.92	0.12	3.39	14.60	0.98	2.14	0.12	14.43	0.1959	0.0040
62	24.40	46.64	0.54	12.07	4.09	0.12	3.45	15.08	1.01	1.96	0.08	14.95	0.1931	0.0029
67	26.40	47.06	0.57	12.65	4.77	0.12	3.43	13.99	1.06	2.15	0.05	14.16	0.2069	0.0041
72	28.40	46.45	0.58	13.19	4.75	0.11	3.51	13.46	0.96	2.22	0.09	14.69	0.2201	0.0040
77	30.40	45.97	0.58	12.60	4.63	0.11	3.68	14.32	1.00	2.12	0.06	14.92	0.2169	0.0037
82	32.40	45.20	0.60	12.77	4.77	0.11	3.75	14.69	1.01	2.14	0.07	14.88	0.2154	0.0046
88	34.80	48.54	0.62	13.67	4.87	0.11	3.71	12.11	1.05	2.26	0.10	12.96	0.2585	0.0043
92	36.40	48.06	0.57	12.59	4.54	0.11	3.55	13.65	1.08	2.11	0.07	13.68	0.2195	0.0042
97	38.40	48.36	0.60	13.31	4.99	0.11	3.50	12.41	1.02	2.25	0.10	13.34	0.2380	0.0041
102	40.40	46.55	0.62	13.40	5.13	0.11	3.46	12.97	1.00	2.31	0.12	14.33	0.2251	0.0044
107	42.40	46.05	0.60	13.13	4.87	0.12	3.47	13.62	1.01	2.22	0.09	14.82	0.2150	0.0044
113	44.80	47.17	0.57	12.88	4.70	0.12	3.56	14.05	1.10	2.08	0.06	13.72	0.2138	0.0040
117	46.40	47.44	0.59	13.13	4.77	0.11	3.42	13.20	1.03	2.19	0.11	14.00	0.2186	0.0043
122	48.40	48.12	0.63	14.28	5.21	0.11	3.37	11.37	1.00	2.35	0.08	13.49	0.2501	0.0039
127	50.40	47.73	0.61	12.51	4.77	0.11	3.54	13.77	1.10	2.20	0.08	13.57	0.2169	0.0042
132	52.40	47.93	0.59	12.36	4.85	0.12	3.54	13.59	1.14	2.10	0.11	13.68	0.2198	0.0038
137	54.40	47.93	0.59	12.91	4.65	0.11	3.33	13.29	1.06	2.12	0.08	13.93	0.2114	0.0040
142	56.40	48.28	0.56	12.34	4.57	0.13	3.49	14.28	1.27	2.01	0.13	12.93	0.2062	0.0037
147	58.40	46.38	0.59	12.58	4.73	0.12	3.37	14.43	0.89	2.09	0.09	14.74	0.1971	0.0036
152	60.40	48.07	0.58	12.56	4.54	0.11	3.28	13.79	1.00	2.05	0.09	13.93	0.2007	0.0038
157	62.40	49.09	0.54	12.05	4.30	0.12	3.32	14.46	1.24	1.94	0.09	13.25	0.1937	0.0041
162	64.40	50.63	0.55	12.50	4.32	0.11	3.29	13.19	1.17	1.97	0.10	12.17	0.2105	0.0038

Table 3
Minor elements in the sediment. Samples position starts from the base of the Enza section.

Sample	Position	Sc	V	Cr	Co	Ni	Cu	Zn	As	Rb	Sr	Y	Zr	Nb	Ba	La	Ce	Pb	Th	S	Br	Mo	TOC
	(m)	(ppm)	(ppm)	(ppm)	(ppm)	(ppm)	(ppm)	(ppm)	(ppm)	(ppm)	(ppm)	(ppm)	(ppm)	(ppm)	(ppm)	(ppm)	(ppm)	(ppm)	(ppm)	(ppm)	(ppm)	(ppm)	(%)
4	1.2	9	94	138	16	80	19	74	7	113	451	19	110	10	281	15	61	14	2	2250	<20	<3	0.56
12	4.4	11	101	143	14	88	35	93	7	114	429	18	96	10	287	22	67	6	2	770	<20	<3	0.52
17	6.4	7	98	134	11	80	18	70	10	114	473	20	105	11	313	35	62	3	9	1910	<20	3	0.5
22	8.4	2	100	114	12	74	23	95	5	103	531	16	67	10	261	38	69	4	12	1430	<20	<3	0.68
27	10.4	10	104	108	11	74	29	103	10	131	578	22	53	13	293	26	62	11	12	750	<20	3	0.69
32	12.4	11	94	136	16	80	22	96	5	118	464	22	128	13	286	24	62	8	10	670	<20	<3	0.46
37	14.4	7	95	132	13	77	33	94	14	131	522	24	106	13	318	22	50	7	7	2890	<20	<3	0.57
42	16.4	9	100	124	11	80	22	94	<3	104	379	17	88	8	266	13	58	7	10	1600	<20	<3	0.67
47	18.4	9	98	128	10	79	23	101	11	120	435	21	101	9	282	21	60	9	15	2990	<20	<3	0.58
52	20.4	4	101	138	11	85	25	100	<3	103	366	14	84	10	290	22	75	9	12	610	<20	3	0.62
57	22.4	12	104	136	16	87	34	98	20	111	419	20	79	9	280	31	60	7	14	3310	<20	3	0.61
62	24.4	16	87	134	14	74	23	82	11	71	317	14	67	9	251	26	56	2	11	1670	<20	<3	0.5
67	26.4	13	102	147	11	87	19	93	21	111	415	18	102	10	280	19	58	2	7	2800	<20	<3	0.46
72	28.4	10	106	141	15	98	23	96	2	115	385	19	93	11	275	25	50	7	12	2580	<20	<3	0.44
77	30.4	7	104	158	13	96	22	99	9	99	374	18	88	12	274	28	69	7	6	2600	<20	<3	0.38
82	32.4	12	106	165	13	88	16	97	13	122	488	23	122	12	283	20	68	10	9	2830	<20	<3	0.42
88	34.8	12	105	166	13	87	19	95	6	114	371	23	165	11	280	29	87	8	9	1590	<20	<3	0.35
92	36.4	13	102	139	10	76	17	88	<3	111	405	23	141	8	297	13	61	11	14	1980	<20	3	0.41
97	38.4	14	109	148	14	85	32	96	5	109	360	22	118	10	318	21	59	4	16	2760	<20	<3	0.41
102	40.4	11	106	126	11	76	17	82	<3	129	407	21	104	13	286	28	81	9	16	1750	<20	3	0.44
107	42.4	11	111	142	13	77	24	101	11	118	429	20	102	10	318	29	73	8	12	1590	<20	<3	0.43
113	44.8	8	101	132	13	71	19	88	16	111	403	21	143	11	289	17	82	10	7	2260	<20	<3	0.39
117	46.4	13	101	132	10	74	17	74	4	122	403	20	129	12	263	29	72	5	10	1600	<20	<3	0.43
122	48.4	13	113	158	12	87	19	101	6	108	313	18	94	10	294	28	75	13	10	2860	<20	<3	0.42
127	50.4	8	100	137	13	79	14	100	9	116	414	26	136	13	321	15	46	11	6	3660	<20	<3	0.39
132	52.4	16	99	139	13	79	19	97	23	103	370	20	107	12	285	28	72	13	7	1890	<20	3	0.44
137	54.4	12	105	141	14	80	22	99	<3	107	384	22	113	10	301	29	58	12	8	2190	<20	3	0.58
142	56.4	13	84	145	10	71	16	60	20	93	377	19	148	12	303	19	67	6	11	3400	<20	<3	0.52
147	58.4	11	96	130	11	72	18	72	13	98	374	16	82	10	275	44	60	10	14	2330	<20	<3	0.48
152	60.4	11	95	137	10	74	28	90	18	99	375	19	118	9	312	41	60	7	2	2610	<20	4	0.48
157	62.4	10	85	154	11	73	27	81	<3	96	425	23	160	8	304	22	70	8	14	5570	<20	3	0.52
162	64.4	13	86	141	10	73	12	61	16	90	361	18	132	10	273	9	73	2	3	4950	<20	4	0.34

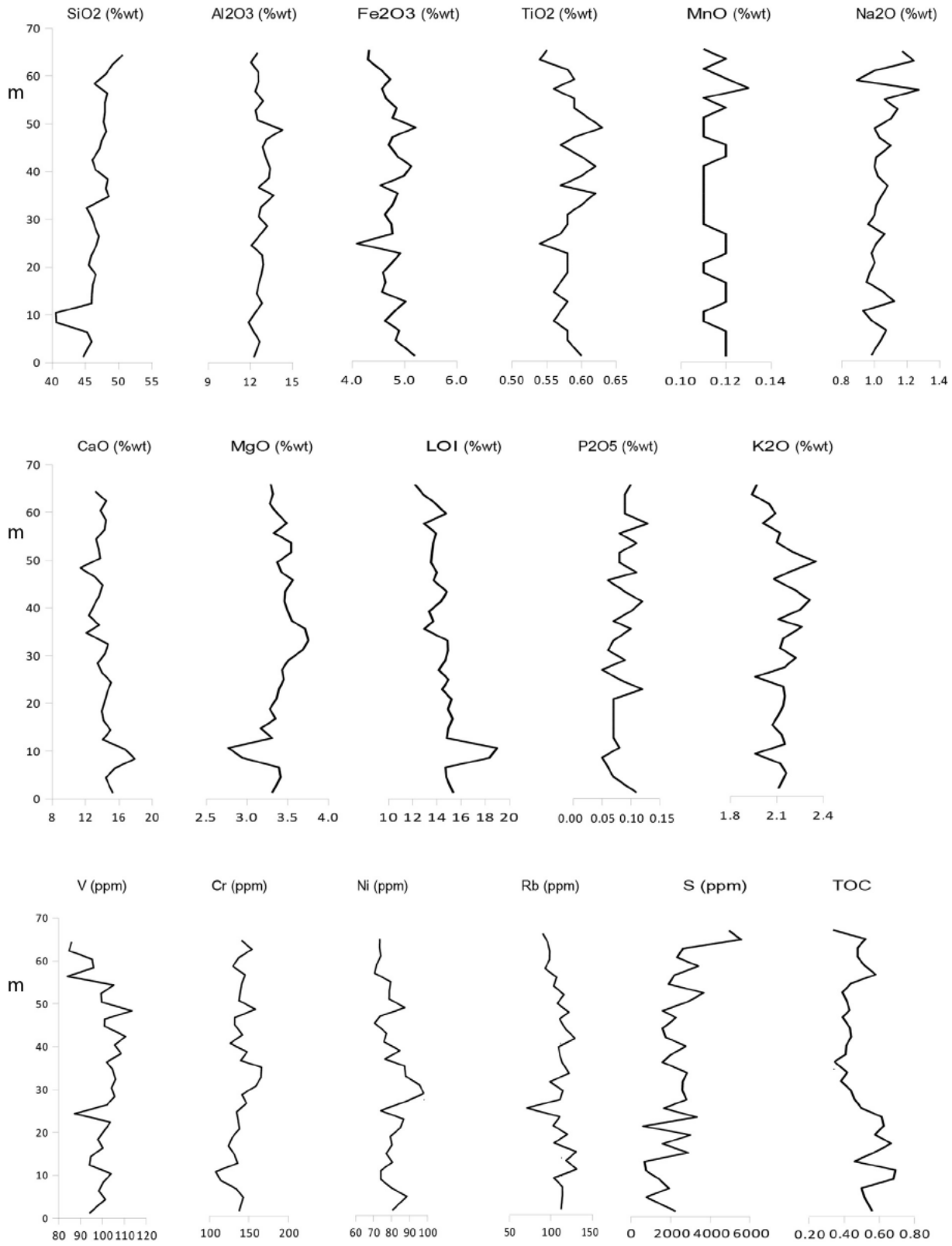

Figure 5. Along-section profiles of major oxides, LOI and minor elements in the sediment of the investigated succession, from the base (1.2 m) to the top (64 m).

of Geosciences and Georesources (CNR IGG) of Pisa and by J. Reitner (personal communication). The sampling for these analyses has been done slicing the carbonates and using a micro-driller to collect the sub samples, in order to have precise measuring of the isotopes in the different areas. The powdered sub samples (100–200 μg) were reacted for 10 min at 90 °C with 100% phosphoric acid on an automated carbonate device connected to a VG PRISM mass spectrometer calibrated with NBS18,

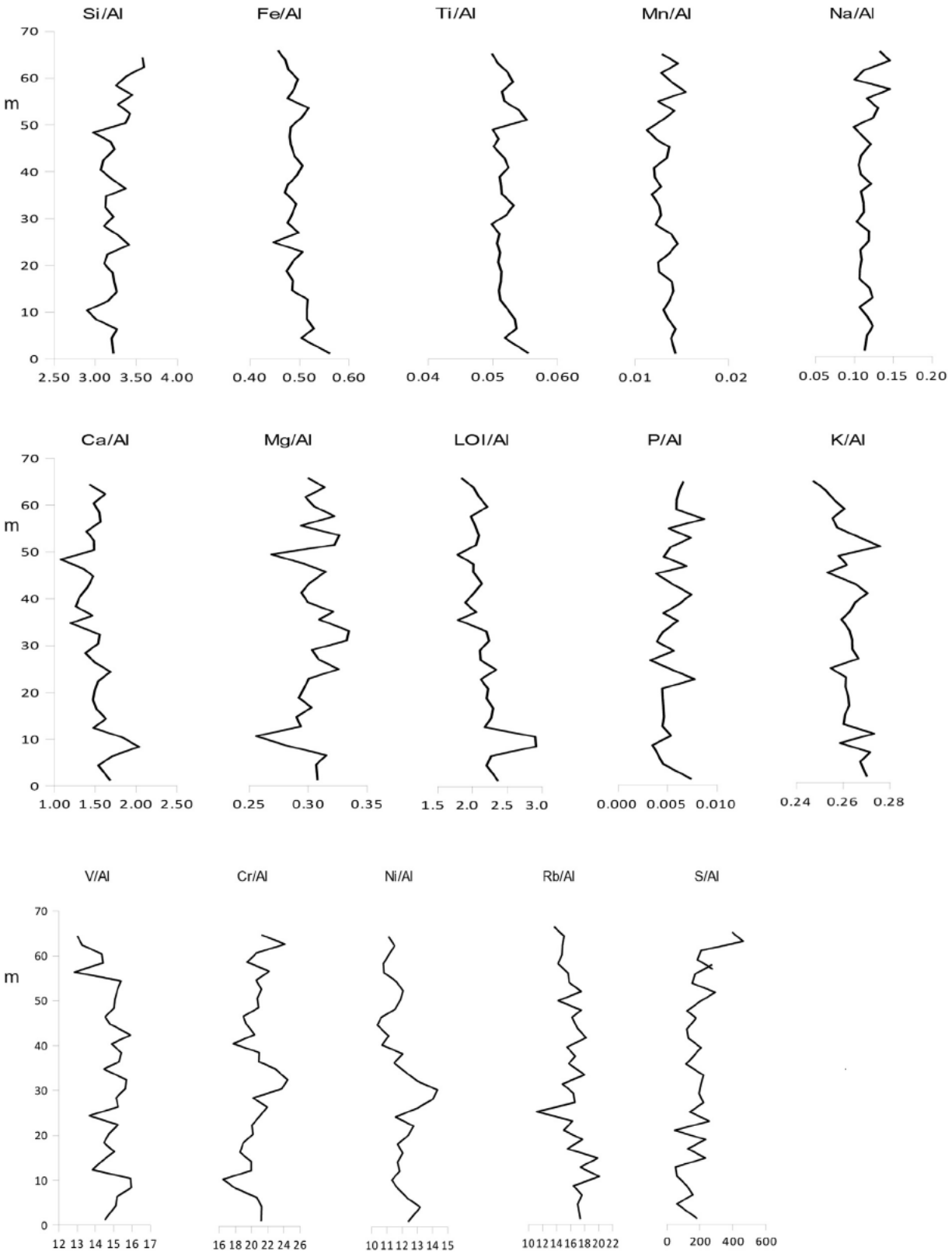

Figure 6. Along-section profiles of elements occurring in the sediment normalized respect to Aluminium.

NBS19 and NBS20 standards. The results are reported in the conventional δ‰ notation with reference to VPDB (Vienna Pee-dee Belemnite). For the dolomite samples (sample with N 20% of dolomite) $\delta^{18}O$ values were calculated with the Rosenbaum and Sheppard fractionation factor. Analytical reproducibility of the method, based on repeated analysis of standards is better than ±0.1‰ for both carbon and oxygen (Rosenbaum, 1994; Rosenbaum and Sheppard, 1986).

Table 4
Mineral abundances in the carbonates concretions.

Sample	Calcite	Dolomite	Detrital
	(%)	(%)	(%)
En5 8A	0	65	35
En5 8B	6	57	37
En5 7A	12	61	27
En5 7B	0	66	34
En5 7C	0	73	27
En5 6A	5	58	37
En5 6B	1	65	34
En5 6C	5	60	35
En5 5A	0	75	25
En5 5B	0	74	26
En5 5C	10	55	35
En5 4A	0	78	22
En5 4B	0	71	29
En5 4C	13	46	41
En5 3A	0	80	20
En5 3B	0	80	20
En5 3C	11	50	39
En5 2A	0	82	18
En5 2B	1	75	23
En5 2C	6	60	34
En5 1A	0	71	29
En10 1A	0	76	24
En10 1B	2	75	22
En10 2A	0	81	19
Cr2A	0	80	20
Cr2B	4	71	25
Cr3A	0	65	35
Cr3B	11	52	37

4. Results

4.1. Hosting sediments geochemistry and mineralogy

XRD analyses (Table 1) show ca. 21% content of carbonate minerals in the sediments, mainly formed of calcite, dolomite is also present (1%) but just in few samples located between 28.4 m and 64.4 m along the section, coupled with the appearance of protodolomite.

The bulk of these carbonates is made of biogenic residuals, mainly foraminifera and calcareous nannoplancton. The other minerals in the Argille Azzurre Fm. sediments of the Enza section are quartz (ca. 20%), clay minerals as smectite and illite (ca. 18%), feldspars (ca. 12%), plagioclase (ca. 9%); muscovite (ca. 8%) and chlorite (ca. 7%). The along section chemical profiles show a clear perturbation around 10 m (Tables 2 and 3; Fig. 5) where a positive peak of CaO, LOI and in part TOC is matched by a negative peak of to SiO_2, Al_2O_3, Fe_2O_3, and K_2O. This is the most evident occurrence, but as other minor peaks in the logs of these elements, reflect the biogenic carbonate/silicate proportion.

MgO displays a peculiar trend with a maxima in the central portion of the log (between 30 and 35 m) and an increasing trend up section. Cr and Ni show a similar trend. TOC has a variable distribution with concentrations around 0.6% up to 22 m, then a decrease around 0.4% up to 52 m and then an increase at the top of the section. The normalisation with respect to Al (Fig. 6) shows that the peaks of SiO_2, Al_2O_3, Fe_2O_3, K_2O, Cr and Ni persist at 10, 25 and 50 m.

Figure 6 shows peaks in the normalized profiles of Cr, Ni and Mg between 30 and 40 m.

4.2. Carbonate geochemistry and mineralogy

Carbonate bodies are mainly composed of dolomite (in average 68% bulk weight) with low and variable amounts of calcite (up to 13%) (Table 4).

The detrital fraction (up to 41%) is similar in all the samples: major components are quartz, feldspars, plagioclase, clay minerals and micas. The concretion Cr3A has also high content of pyrite and arsenopyrite (5%) and is the only sample where strontianite is present (1%).

Table 5
Major oxides in the carbonate concretions.

Sample	SiO_2	TiO_2	Al_2O_3	Fe_2O_3	MnO	MgO	CaO	Na_2O	K_2O	P_2O_5	LOI	Mg/Ca	Sr/Ca
	(wt %)	(wt %)	(wt %)	(wt %)	(wt %)	(wt %)	(wt %)	(wt %)	(wt %)	(wt %)	(wt %)		
En5 8A	12.94	0.17	3.46	1.83	0.09	17.98	25.26	0.55	0.58	0.09	37.06	0.6007	0.0018
En5 8B	21.53	0.26	6.04	2.68	0.13	13.32	23.47	0.66	0.94	0.09	30.87	0.4789	0.0018
En5 7A	14.95	0.18	3.72	1.86	0.09	17.34	24.01	0.60	0.63	0.09	36.53	0.6094	0.0021
En5 7B	14.47	0.18	4.02	1.78	0.10	17.52	24.56	0.60	0.62	0.08	36.08	0.6020	0.0016
En5 7C	16.60	0.23	4.75	2.18	0.11	15.36	25.54	0.57	0.77	0.11	34.77	0.5075	0.0018
En5 6A	13.34	0.19	3.67	1.84	0.09	18.02	24.91	0.52	0.63	0.06	36.73	0.6104	0.0017
En5 6B	12.74	0.18	3.75	1.73	0.09	17.97	25.07	0.53	0.60	0.07	37.27	0.6049	0.0018
En5 6C	16.94	0.20	4.22	2.16	0.11	15.63	24.59	0.60	0.72	0.10	34.73	0.5364	0.0023
En5 5A	14.91	0.19	3.89	1.87	0.10	17.47	24.40	0.58	0.66	0.10	35.83	0.6042	0.0020
En5 5B	16.54	0.21	4.24	2.00	0.10	16.82	24.05	0.59	0.74	0.12	34.58	0.5902	0.0022
En5 5C	23.32	0.27	6.05	2.95	0.13	12.92	22.96	0.66	0.98	0.08	29.68	0.4748	0.0023
En5 4A	14.52	0.18	3.72	1.81	0.10	17.65	24.67	0.54	0.63	0.11	36.07	0.6037	0.0018
En5 4B	15.40	0.18	3.81	1.77	0.10	17.37	24.41	0.58	0.66	0.10	35.61	0.6005	0.0023
En5 4C	24.95	0.29	6.41	3.23	0.15	11.84	23.08	0.72	1.03	0.14	28.15	0.4329	0.0019
En5 3A	15.00	0.19	4.08	1.84	0.10	17.41	24.47	0.61	0.63	0.10	35.58	0.6004	0.0022
En5 3B	17.01	0.19	3.92	1.89	0.10	16.80	24.32	0.66	0.68	0.11	34.33	0.5829	0.0019
En5 3C	25.96	0.29	6.62	3.12	0.14	11.50	22.68	0.74	1.07	0.10	27.78	0.4279	0.0017
En5 2A	13.08	0.18	3.77	1.69	0.09	17.80	25.11	0.54	0.62	0.08	37.03	0.5982	0.0020
En5 2B	15.62	0.19	3.93	1.70	0.09	17.20	24.46	0.66	0.65	0.11	35.40	0.5934	0.0022
En5 2C	22.81	0.26	5.92	2.80	0.14	12.48	24.01	0.74	0.94	0.09	29.84	0.4386	0.0020
En5 1A	19.66	0.26	5.62	2.56	0.12	14.00	23.46	0.62	0.90	0.10	32.70	0.5036	0.0014
En10 1A	14.79	0.20	4.36	1.78	0.10	17.13	23.90	0.37	0.57	0.21	36.59	0.5680	15.2939
En10 1B	21.75	0.27	6.08	2.40	0.11	13.45	22.31	0.50	0.85	0.20	32.07	0.6585	11.1116
En10 2A	16.78	0.21	4.59	2.05	0.11	16.07	23.85	0.45	0.61	0.23	35.05	0.4833	21.6196
Cr2A	25.40	0.28	6.04	2.46	0.15	12.95	22.80	0.68	0.84	0.14	28.26	0.6379	6.0197
Cr2B	26.93	0.24	5.80	2.12	0.11	14.04	21.32	0.82	0.73	0.23	27.66	0.7167	15.6611
Cr3A	14.14	0.27	5.60	8.94	0.26	13.19	27.29	0.92	0.78	1.30	27.33	0.6029	18.8705
Cr3B	25.47	0.27	5.27	2.60	0.14	16.86	26.43	0.73	0.75	0.32	21.16	0.6738	19.5430

Dolomite content increases toward the internal parts of the chimneys, whereas in the external portion the calcite cement and the detrital fraction are more abundant. Terrigenous components, such as SiO_2, Al_2O_3 and Fe_2O_3, increase towards the external areas; whereas, elements pertaining to the carbonate phases have their maximum in the middle and internal parts (Table 5; Fig. 7).

The trace elements Cr, V, Ni and Rb show maximum concentrations in the external parts of the chimney, while S has a small

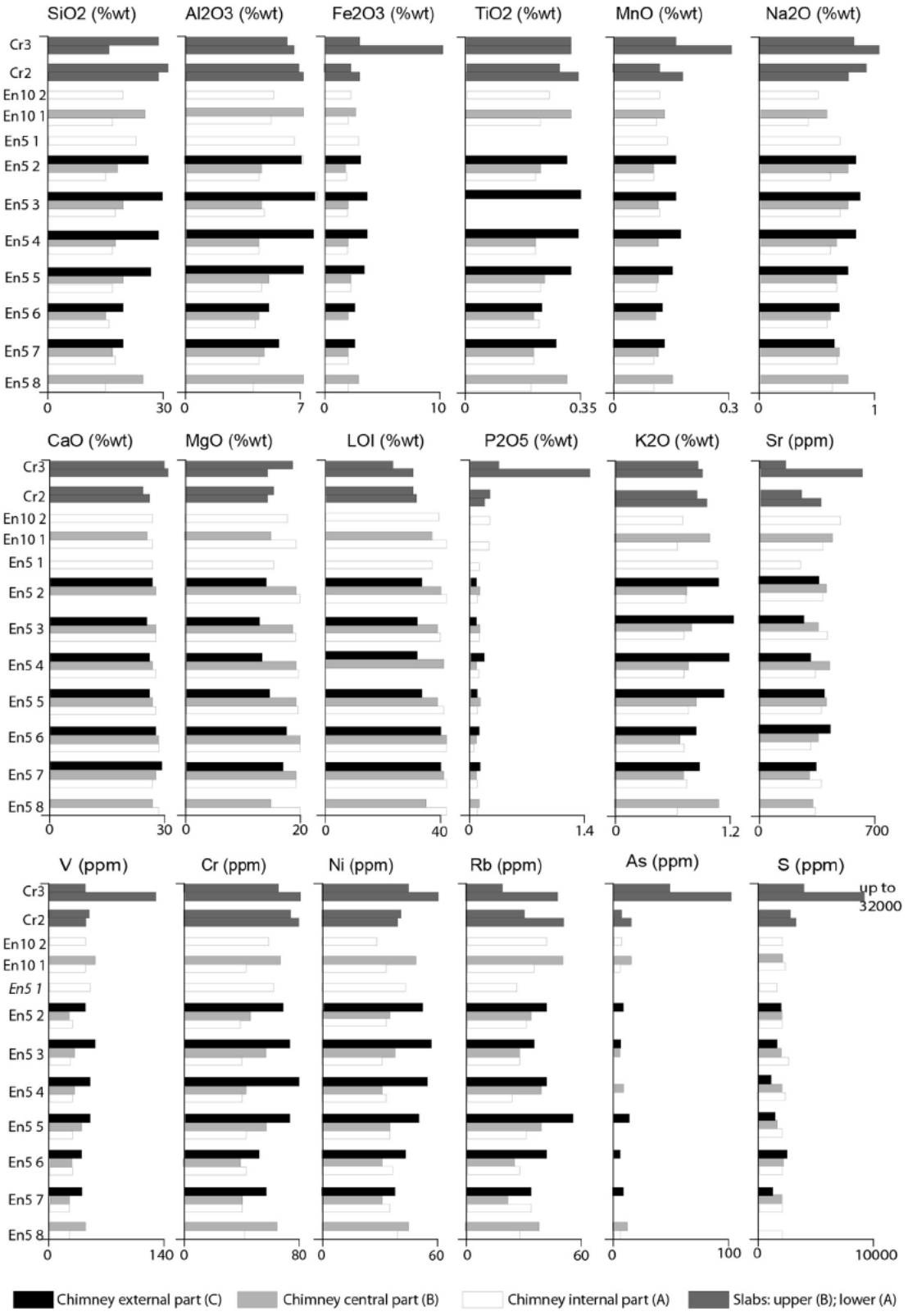

Figure 7. Major oxides concentration, LOI and minor elements of the carbonate chimneys (En5 En10), slab (Cr2) and the concretion (Cr3).

Table 6
Minor elements in the carbonate concretions.

Sample	V	Cr	Co	Ni	Cu	Zn	As	Rb	Sr	Y	Zr	Nb	Ba	La	Ce	Pb	Th	S	TOC
	(ppm)	(ppm)	(ppm)	(ppm)	(ppm)	(ppm)	(ppm)	(ppm)	(ppm)	(ppm)	(ppm)	(ppm)	(ppm)	(ppm)	(ppm)	(ppm)	(ppm)	(ppm)	(%)
En5 8A	24	35	<3	34	6	34	5	23	320	2	2	2	223	12	23	<3	<3	1950	0.48
En5 8B	40	56	<3	39	4	26	10	32	308	3	17	7	300	12	40	<3	<3	1060	0.60
En5 7A	22	36	<3	30	4	32	<3	30	356	3	2	6	264	<3	22	<3	6	2330	0.24
En5 7B	21	36	<3	27	12	29	<3	18	286	3	2	5	235	11	47	<3	7	2150	0.22
En5 7C	36	51	<3	33	12	40	10	29	332	2	2	6	269	4	39	<3	5	1380	1.00
En5 6A	26	39	<3	32	7	34	<3	25	301	2	2	8	250	<3	25	<3	<3	2250	0.45
En5 6B	24	35	<3	27	14	33	<3	22	331	2	2	5	258	11	31	<3	<3	2450	0.93
En5 6C	33	43	<3	38	10	39	5	36	413	2	2	6	250	10	53	<3	7	2660	0.36
En5 5A	27	37	<3	31	9	38	<3	26	349	5	2	5	245	9	44	<3	3	2160	0.67
En5 5B	32	50	<3	30	14	37	<3	33	384	4	2	6	273	9	37	<3	4	1850	0.26
En5 5C	44	65	4	45	10	51	13	48	380	7	19	9	278	18	37	<3	7	1590	0.40
En5 4A	26	35	<3	29	10	35	<3	21	310	4	2	6	243	<3	28	<3	4	2590	1.13
En5 4B	27	38	<3	27	6	35	7	34	397	3	2	6	259	4	25	<3	5	2061	0.77
En5 4C	45	70	<3	47	17	50	<3	36	310	3	6	5	296	13	33	<3	7	1340	0.29
En5 3A	23	35	<3	27	8	31	<3	24	376	5	2	4	272	9	25	<3	<3	2880	0.20
En5 3B	27	48	<3	33	6	36	4	24	334	5	2	3	258	<3	33	<3	5	2280	0.22
En5 3C	50	64	4	49	19	51	7	30	269	6	16	5	259	6	54	<3	8	1830	0.35
En5 2A	26	34	<3	29	10	35	<3	26	365	2	2	6	223	<3	31	<3	<3	2390	1.02
En5 2B	20	40	<3	30	6	33	<3	29	388	2	4	4	251	3	32	<3	10	1940	0.22
En5 2C	40	61	4	44	21	47	8	36	352	10	13	6	284	26	43	<3	4	1910	1.39
En5 1A	42	55	<3	37	17	44	<3	23	239	5	2	4	255	12	37	<3	<3	1750	0.49
En10 1A	39	36	<3	30	14	16	4	30	374	6	17	5	202	10	32	12	4	2520	
En10 1B	49	58	<3	42	13	25	13	44	421	10	39	7	253	3	26	15	<3	2270	
En10 2A	37	52	<3	25	9	16	5	36	466	10	34	5	251	9	13	11	<3	2380	
Cr2A	41	71	<3	34	8	23	14	45	349	11	73	4	284	<3	3	13	<3	3560	
Cr2B	46	67	<3	35	8	22	5	27	237	7	65	3	201	3	26	10	<3	3070	
Cr3A	116	71	22	53	15	42	87	42	590	21	20	7	241	4	35	92	<3	32,000	
Cr3B	40	58	4	39	12	20	41	17	159	3	36	<3	202	<3	<3	20	<3	4390	

increase in the internal areas. The overall content of trace elements is higher in samples En5 with respect to samples En10.

The slab (sample Cr2) and the concretion (Cr3) consist of dolomite (up to 80% wt), whereas calcite is present in correspondence of the white zone of Cr2B (4% wt) and in the carbonate fraction of Cr3B (11% wt) (Table 4). MgO is usually higher in the chimneys than in the slabs. These latter, on the other hand, show higher concentrations of V, Cr, and S.

Cr3A shows higher concentrations of trace elements than Cr2 and Cr3B (Fig. 7). For instance S reaches the concentration of 32,000 ppm in Cr3A (Table 6). Furthermore, this sample has the lowest concentration of SiO_2.

4.3. Carbonate stable isotopes

In Table 7 are presented the results for the $\delta^{13}C$ and $\delta^{18}O$ for carbonate samples. The slabs show carbon isotope values more depleted than chimneys, in particular Cr3A is the most negative with −40.13‰ VPDB.

$\delta^{13}C$ values are generally more negatives toward the internal parts (A) of the En5 chimney, ranging between −17.07 and −20.06‰ VPDB, respect to the $\delta^{13}C$ of −8.6‰ VPDB, detected in the externals parts in the sample En5_3C. A further variation of ^{13}C has been observed from the top (En5_8) to the bottom (En5_1) of the chimney showing less negative $\delta^{13}C$ values. The $\delta^{18}O$ isotope values range between 4.37‰ and 6.24‰ VPDB. In this case the slabs values, ranging between 4.4‰ and 6.24‰ VPDB, are close to those from the chimneys, which are between 4.37‰ and 6.21‰ VPDB.

4.4. Carbonate petrography

Petrographic observation of thin sections was performed along En5 chimney, on the Cr3A dark concretion and on the carbonate breccia enclosed in the rhodolith rich layer.

- The EN5 chimney is cemented by dolomitic micrite (hereafter referred to as dolomicrite) and microsparite (Figs. 8A and 9A) with abundant angular to sub angular quartz clasts (up to 35% vol., 50–150 μm). SEM EDS analyses revealed the presence of clusters of framboidal pyrite engulfed within the dolomitic cements (Fig. 9B). The chimney shows clear zonation probably due to dissolution–cementation cycles (Fig. 8 B–C). This zonation is marked by corrosion surfaces often lined by a thin generation (ca. 10 μm) of isopachous scalenohedral calcite (Fig. 8B–C). Locally, the chimneys are made of alternating peloidal micrite and dolomicrite. Peloids are 250–500 μm ovoidal to circular in shape, organized in clotted fabric (Fig. 8D); inter peloids porosity is filled with microcrystalline cements and sand sized clasts of quartz. Thin levels (ca. 500 μm) of sandy dolomicrite are breached by sigmoidal fractures (Fig. 8 E–F). Well rounded clasts of glauconite (Figs. 8C and 9C) are sparse in the matrix as well as poorly rounded mica and plagioclase crystals. The chimneys are often breached by systems of radial and longitudinal fractures partially filled by microsparite (Fig. 8F). Some of those networks show geometrical intersections that suggest a likely affinity with tension cracks structures (Fig. 8G).
- *Dark limestone* (sample Cr3A), which stratigraphically overlies the chimneys, is made of micrite with clasts of quartz (>50% vol., 50–150 μm) and mottled micrite that shows peloidal fabric. Toward the upper surface of the slab, this facies is bounded by red coralline algae (Fig. 8H). Rhodalgal coated chips of fossil barren mudstone together with foraminifera and coral re mains are shown in Figure 8I.
- *In situ carbonate breccia* is made of millimetre sized pebbles of micrite, micrite with abundant sand sized clasts of quartz and red algae fragments. Several centimetre sized rhodolithes were described within this facies (Fig. 8J). This facies show high voids ratio; sometimes voids are filled by mesosparite and botryoids of acicular aragonite (Fig. 8J). An isopachous generation of scalenohedral calcite growth on the carbonatic pebbles. Macro borings are restricted to the rhodolithes, indicating lithification before the settlement of macroborers (Fig. 8 K–L). Macroborings are filled with bright luminescence micrite, with sand sized clasts of quartz and probably feldspar (Fig. 8 K–L)

5. Discussion

The chemical composition of the Argille Azzurre Fm. that hosts the seep carbonates reflects the mineralogy of the eroded rocks supplying sediments to the continental shelf during the Pleistocene (Capozzi and Picotti, 2010; Capozzi et al., 2012; Dinelli et al., 2012). Elements linked with quartz, plagioclase, micas, clay minerals and feldspars are abundant. The enrichment of Ni and Cr indicates the presence of mafic and ultramafic minerals, derived from the contribution of local magmatic rocks occurring within the drainage area in the emerging Northern Apennines chain (Picotti et al., 2007; Ghielmi et al., 2010; Gunderson et al., 2014). The enrichment in CaO, LOI and TOC matched by a negative peak of SiO_2, Al_2O_3, Fe_2O_3, and K_2O at 10 m seems to be associated to the presence of a thin horizon probably corresponding to a peak of primary productivity, linked to calcareous phytoplankton and associated with organic carbon. Negative peaks of Al_2O_3, Fe_2O_3, K_2O, TiO_2, V and Rb (Fig. 5), coupled with the positive peak of Si/Al (Fig. 6) at 25 m suggest a grain size increase, corresponding to the occurrence of thin sandy and silty sand layers in the succession, coupled with the first occurrence of carbonate concretions. The same variations can be found at 50 m, where the sandy layers are well developed and thicker slabs occur along the bedding planes (Oppo et al., in this isue). The carbonate minerals in the sediments are mainly attributed to the presence of fossil tests. However, dolomite and protodolomite occur only in the upper 35 m of the section, suggesting an origin linked to the same processes that generated the associated carbonate concretions.

The concretions are mainly composed of authigenic dolomite (>60% wt), variable amounts of calcite (<15% wt) and detrital fraction. The cements petrography frequently shows clotted peloidal micrite. This microfabric has been widely observed in methane derived authigenic carbonates (MDAC) found in active or fossil cold seep systems (e.g. Peckmann et al., 2001; Magalhaes,

Table 7
Stable isotopes in the carbonate concretions. The symbol * indicates the measurements performed at CNR-IGG in Pisa.

Sample	$\delta^{13}C$ (vpdb)	$\delta^{18}O$ (vpdb)
En5 8A	−20.06	5.86
En5 8B	−19.49	5.47
En5 6A	−19.31	6.2
En5 6B	−18.97	6.13
En5 4A*	−18.22	6.08
En5 3A	−18.61	6.21
En5 3C	−8.60	4.37
En5 1A	−17.07	5.59
En5 1B	−16.07	5.49
Cr2A*	−28.56	6.12
Cr3A	−35.42	4.49
Cr3A	−40.13	4.44
Cr3A*	−30.69	5.10
Cr3B* (calcite)	−30.91	5.44
Cr3B*	−35.39	6.13
Cr3B* (calcite + dolomite)	−35.07	6.24

2007; Capozzi et al., 2012). The peloids are interpreted as the product of intense and widespread microbial activity during carbonate precipitation (Peckmann et al., 2001; Peckmann and Thiel, 2004; Peckmann et al., 2007; Feng et al., 2008). Sulphur is particularly abundant in Cr3A and reflects the occurrence of pyrite and arsenopyrite. Further evidence of AOM can be found in the stable isotope ratios of the carbonate cements (Table 7). In the chimneys of Enza River, the $\delta^{13}C$ ranges between 8.60‰ and 20.06‰(VPDB), whereas the slabs have lower values, ranging between 28.56‰ and 40.13‰ VPDB. These values are indicative of AOM processes, as described for MDAC elsewhere (e.g. Rodriguez et al., 2000; Diaz del Rio et al., 2003; Hensen et al., 2007; Capozzi et al., 2012; Magalhaes et al., 2012). The $\delta^{18}O$ in our samples vary from 4.4‰ VPDB and 6.2‰ VPDB meaning that they are significantly enriched in ^{18}O with respect to carbonates precipitated in a nowadays seawater conditions where $\delta^{18}O$ is usually between 0‰ and 1‰ VPDB (Magalhaes, 2007). This enrichment could be explained by the fact that carbonate dolomite phase shows usually an increase of 2–4‰ in $\delta^{18}O$ composition respect to the ambient water (Budd, 1997; Aloisi et al., 2000; Oppo et al., in this issue); moreover according to Zachos et al., 2001 the values of $\delta^{18}O$ during the Early Pleistocene were around 3‰ VPDB (Oppo et al., in this

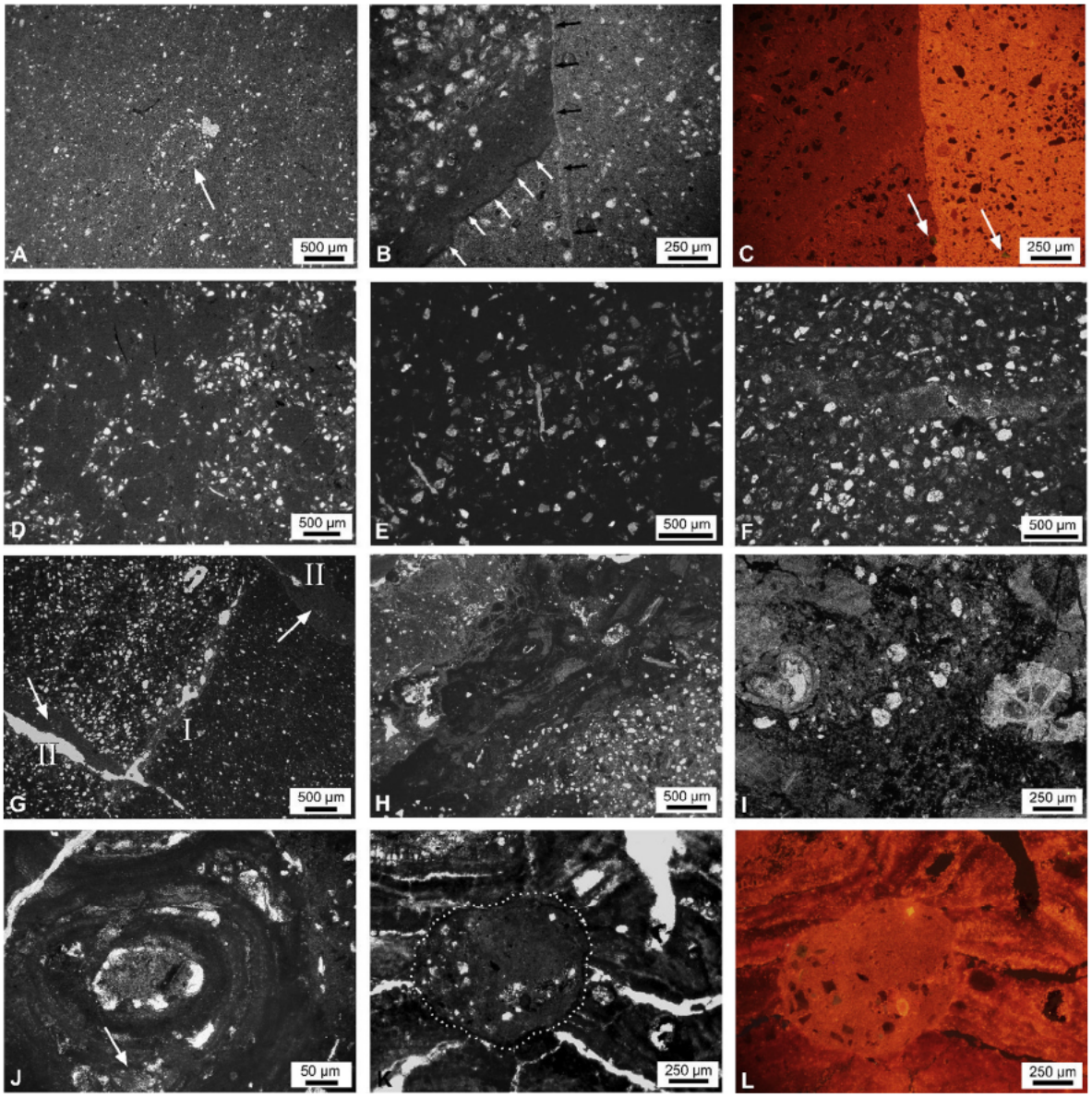

Figure 8. Photomicrographs of the studied carbonates. A) Mottled micrite/microsparite with abundant angular to sub-angular quartz clasts. The arrow point to a rounded carbonate intraclast fouled by angular quartz clasts. B) Fractures (bright cements) breaching the chimney dolomicrite (darker cements). Often fracture walls are lined by dark layers of organic matter-rich micrite (with arrows) or thin isopachous generation of calcite cements (black arrows). C) Cathodoluminescence photomicrograph (same as B) showing two dominant phases: bright luminescent fracture fills, dominated by calcitic micrite; dark red dolomicrite. Arrows point to glauconite clasts. D) Peloidal fabric within chimney wall. Note that peloids are avoid of quartz clasts. E) Thin layer of angular quartz clasts breached perpendicularly by hollow fractures. F) Fractures filled by microcrystalline cements. G) Two perpendicular systems of fractures: first system (I), parallel to the chimney's wall, mark the contact between dolomitic sandstone (upper left) and dolomicrite (lower right); the second system (II), perpendicular to the first one, is partially filled by micrite (arrows). H, I) Topmost part of the dark concreted slab showing red algae bounding dolomitic sands. Red algae level is covered by thin bioclastic mud with rare quartz clasts (upper left in H). J) Red algal rhodoids. Large voids within the thallus (conceptacles) are locally filled with aragonite (arrow). K L) Macroboring (dotted line) within red algal rhodoids is infilled with bright luminescence sandy micrite (L). (For interpretation of the references to colour in this figure legend, the reader is referred to the web version of this article.)

issue). Petrographic analyses revealed that the chimneys are breached by expansion and sigmoidal fractures that have been described elsewhere within gas saturated sediments (Mazzini et al., 2005) and might be related to fluids expulsions related processes. This fracture network would represent the main mechanism of gas diffusion in fine grained sediments as observed in the model of Choi et al. (2011).

The progressive increase of carbonate cements is observed to ward the internal parts of the chimneys, which is mainly made of dolomite (up to 82% bulk rock in the sample En5_2A). Otherwise, authigenic calcite increases in the external parts. The higher content of calcite toward the edges reflects the increased influence of pore water rich of SO_4^{2-}, which inhibits the dolomite precipitation in anaerobic environment and favours the formation of calcite (e.g. Douglas, 2005).

Higher concentration of SiO_2 and Al_2O_3 in the external areas of the EN5 evidence the gradual increase of siliciclastics from the internal to external areas, as suggested by the changes in mineralogy.

The chimneys form due to the focused fluids flow through a narrow discontinuity in the sediment interval consistent with the increase of sand within sedimentary record. The continued and vigorous flow progressively displaces the sediment particles and creates an open central vent that in some cases has been fully closed. The mainly dolomitic phase in cements suggests that all carbonate concretions so far analysed formed within the sediment pile near the Sulphate–Methane Interface (SMI) where the interstitial water is quite depleted in the sulphate component (Magalhaes, 2007; Magalhaes et al., 2012 and references therein).

The enrichment of Fe, S, Ni and Cr, involved in the formation of sulphide minerals in the Cr3A, could indicate precipitation/

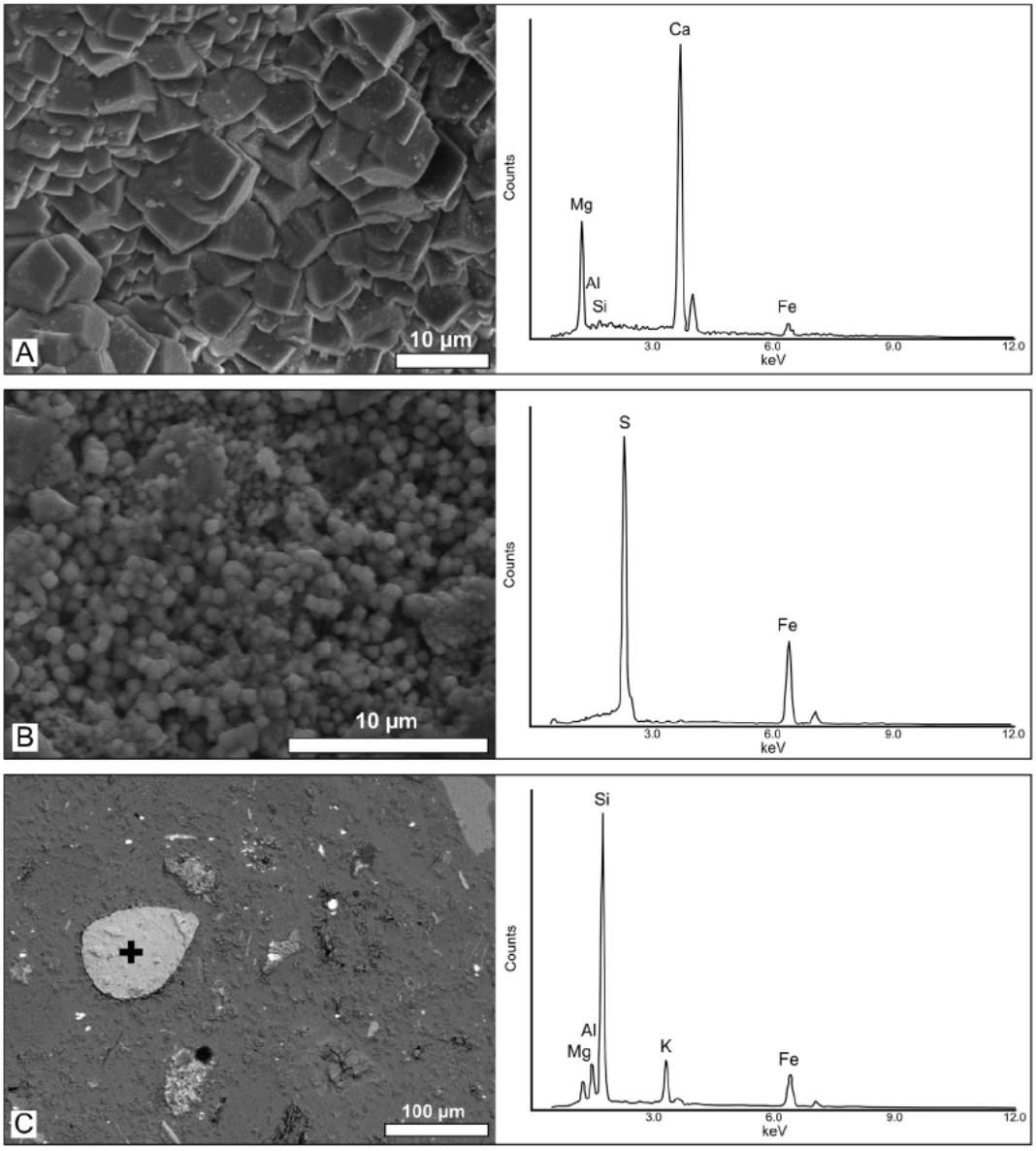

Figure 9. Scanning electron microscope (SEM) photomicrographs and EDX analyses of the dolomitic chimneys from the Enza river. A) Microcrystalline euhedral rhombs of dolomite and EDX spectrum collected with 15 keV accelerating voltage from the entire area. B) Loose euhedral S Fe-rich microcrystals (pyrite). EDX spectrum collected with 15 keV accelerating voltage from the entire area. C) Back scattered (BEI) photomicrograph of chimney dolomicrite showing well rounded clast of glaukonite. EDX spectrum collected with 15 keV accelerating voltage from the bright rounded clast (cross).

alteration of the carbonate by a renewed fluids leakage, permeating the rhodolith enriched layer, after a period of non deposition or erosion at the seafloor. The mottled micrite with its peloidal fabric indicates a renewed bacterial activity that possibly developed near the seafloor. In fact, in situ carbonate breccia also shows high voids ratio in same cases filled by mesosparite and botryoids of acicular aragonite that are very similar to those reported in methane-derived authigenic carbonates recovered at the seafloor in the Black Sea and Adriatic Sea (Naudts et al., 2008; Capozzi et al., 2012).

6. Conclusions

Geochemical analyses on the Argille Azzurre Fm. sediments that host the carbonate concretions revealed their dominant siliciclastic composition, with small contents of biogenic calcite. Dispersed dolomite and protodolomite occur in the upper half of the section in association with the carbonate concretions.

Dolomite cement represents the 60–80 % weight of the studied carbonate concretions. Therefore, the chimney palisade share compositional similarities with analogue dolomitic pipes identified in the Gulf of Cadiz (Magalhaes et al., 2012), southern New Zealand continental slope (Orpin, 1997), offshore Brazil (Wirsig et al., 2012), Black Sea (Reitner et al., 2005), Mediterranean Sea (Angeletti et al., in this issue) and other localities on land (e.g. De Boever et al., 2006a; Cau et al., in this issue).

Petrographic observations support the role of methane enriched fluids in the genesis of the carbonate chimneys and slabs. The occurrence of clotted and peloidal microfabric, which commonly represents bacterially induced precipitates, is frequently observed in methane derived authigenic carbonates. Moreover, stable carbon isotope ratios in cements indicate anaerobic oxida tion of methane and sulphate reduction during the carbonate precipitation.

The dolomite increase in the internal zone of chimneys reflects the progressive isolation from the SO_4 rich pore water, which instead favours the calcite precipitation in the external area. The siliciclastic content increases moving from the internal to external zones due to the sediment displacement operated by the fluid flow along the central emission vent.

Pyrite, arsenopyrite and strontianite together with aragonite botryoids, possibly indicate secondary carbonate dissolution/precipitation within the rhodolith rich bed. The presence of this sul phide within carbonates points to a change in fluid leakage conditions within more permeable sediments saturated by SO_4 rich marine water. These carbonates probably deposited after a period of seabed erosion in the Early Pleistocene shelf environment. The fluid leakage persists in present day, after the emersion of the Apennine foothills.

Acknowledgements

Funding was provided by the national project PRIN 2009 “Carbonate conduits linked to hydrocarbons enriched seepages” (PI R. Capozzi) of the Italian Ministry of University and Research (MIUR). Thanks are due to C. Mazzoli (University of Padua) for the access at the cathodoluminescence facilities. The authors are indebted with two anonymous reviewers for their constructive criticism. This is ISMAR Bologna scientific contribution number 1851.

References

Aloisi, G., Pierre, C., Rouchy, J.-M., Foucher, J.-P., Woodside, J., 2000. Methane-related authigenic carbonates of eastern Mediterranean Sea mud volcanoes and their possible relation to gas hydrate destabilisation. Earth Planet. Sci. Lett. 184, 321 338.

Angeletti, L., Canese, S., Franchi, F., Montagna, P., Reitner, J., Walliser, E.O., Taviani, M., 2015. The chimney forest of the deep Montenegrin margin, south-eastern Adriatic Sea. In: Capozzi, R., Negri, A., Reithner, J., Taviani, M. (Eds.), Carbonate Conduits Linked to Hydrocarbon-enriched Fluid Escape. Special Issue of Mar. and Petr. Geo.

Boccaletti, M., Corti, G., Martelli, L., 2010. Recent and active tectonics of the external zone of the Northern Apennines (Italy). Earth Sci. 100, 1331 1348.

Boetius, A., Ravenschlag, K., Schubert, C.J., Rickert, D., Widdel, F., Giesecke, A., Amann, R., Jorgensen, B.B., Witte, U., Pfannkuche, O., 2000. A marine microbial consortium apparently mediating anaerobic oxidation of methane. Nature 407, 623 626.

Budd, D.A., 1997. Cenozoic dolomites of carbonate islands: their attributes and origin. Earth Sci. Rev. 42, 1 47.

Capozzi, R., Picotti, V., 2010. Spontaneous fluid emissions in the Northern Apennines: geochemistry, structures and implications for the petroleum system. In: Goffey, G.P., Craig, J., Needham, T., Scott, R. (Eds.), Hydrocarbons in Contractional Belts, Geol. Soc London Spec. Publ. 348, London, pp. 115 135.

Capozzi, R., Guido, F.L., Oppo, D., Gabbianelli, G., 2012. Methane-Derived Authigenic Carbonates (MDAC) in northern-central Adriatic Sea: relationships between reservoir and methane seepages. Mar. Geol. 332 334, 174 188.

Capozzi, R., Negri, A., Reitner, J., Taviani, M., Franchi, F., Oppo, D. (Eds.), 2013. Car-bonate Conduits Linked to Hydrocarbon-enriched Fluid Escape, Workshop and Field Seminar, Bologna, June 28th July 1st, 2013, Field Guide and Abstracts with Program, Bologna, pp. 1 51.

Cau, S., Franchi, F., Roveri, M., Taviani, M., 2015. The Pliocene-age Stirone river hydrocarbon chemoherm complex (Northern Apennines, Italy). In: Capozzi, R., Negri, A., Reithner, J., Taviani, M. (Eds.), Carbonate Conduits Linked to Hydrocarbon-enriched Fluid Escape. Special Issue of Marine and Petroleum Geology.

Choi, J., Mouillesseaux, K., Wang, Z., Fiji, H.D., Kinderman, S.S., Otto, G.W., Geisler, R., Kwon, O., Chen, J.N., 2011. Aplexone targets the HMG-CoA reductase pathway and differentially regulates arteriovenous angiogenesis. Development 138, 1173 1181.

Clari, P., Cavagna, S., Martire, L., Hunziker, J., 2004. A miocene mud volcano and its plumbing system: a chaotic complex revised (Monferrato, NW Italy). J. Sediment. Res. 74, 662 676.

De Boever, E., Swennen, R., Dimitrov, L., 2006a. Lower Eocene carbonate-cemented “chimney” structures (Varna, Bulgaria) - control of seepage rates on their formation and stable isotopic signature. J. Geochem. Explor. 89, 78 82.

De Boever, E., Swennen, R., Dimitrov, L., 2006b. Lower Eocene carbonate cemented chimneys (Varna, NE Bulgaria): formation mechanisms and the (a)biological mediation of chimney growth? Sediment. Geol. 185, 159 173.

Díaz-del-Rio, V., Somoza, L., Martinez-Frias, J., Hernandez-Molina, F.J., Lunar, R., Fernandez-Puga, M.C., Maestro, A., Terrinha, P., Llave, E., Garcia, A., Garcia, A.C., Vazquez, J.T., 2001. Carbonate chimneys in the Gulf of Cadiz: initial report of their petrography and geochemistry. In: Akhmanov, G., Suzyumov, A. (Eds.), Geological Processes on Deep-water European Margins. IOC-UNESCO Workshop Report 175, pp. 53 54.

Díaz-del-Río, V., Somoza, L., Martínez-Frías, J., Mata, P., Delgado, A., Hernández-Molina, F.J., Lunar, R., Martín-Rubí, J.A., Maestro, A., Fernández-Puga, M.C., León, R., Llave, E., Medialdea, T., Vázquez, J.T., Hernández-Molina, F.J., 2003. Vast fields of hydrocarbon derived carbonate chimneys related to the accretionary wedge/olistostrome of the Gulf of Cadiz. Mar. Geol. 195, 177 200.

Dinelli, E., Ghosh, A., Rossi, V., Vaiani, S.C., 2012. Multiproxy reconstruction of Late Pleistocene–Holocene environmental changes in coastal successions: micro-fossil and geochemical evidences from the Po Plain (Northern Italy). Stratig-raphy 9, 153 167.

Douglas, S., 2005. Mineralogical footprints of microbial life. Am. J. Sci. 305, 503 525.

Feng, D., Chen, D.F., Qi, L., Roberts, H., 2008. Petrographic and geochemical characterization of seep carbonate from Alaminos Canyon, Gulf of Mexico. Chin. Sci. Bull. SP Science in China Press 53 (11), 1716 1724.

Franzini, M., Leoni, L., Saitta, M., 1972. A simple method to evaluate the matrix effects in X-Ray fluorescence analysis. X-Ray Spectrom. 1, 151 154.

Franzini, M., Leoni, L., Saitta, M., 1975. Revisione di una metodologia analitica per fluorescenza-X, basata sulla correzione completa degli effetti di matrice. Rend. Soc. Ital. Mineral. Petrol. 31, 365 378.

Ghielmi, M., Minervini, M., Nini, C., Rogledi, S., Rossi, M., Vignolo, A., 2010. Sedimentary and tectonic evolution in the eastern Po-Plain and northern Adriatic Sea area from Messinian to Middle Pleistocene (Italy). Rend. Lincei 21, S131 S166.

Goldsmith, J.R., Graf, D.L., 1958. Relation between lattice constants and composition of the Ca Mg carbonates. Am. Mineral. 43, 84 101.

Gunderson, K.L., Pazzaglia, F.J., Picotti, V., Anastasio, D.A., Kodama, K.P., Rittenour, T., Frankel, K.F., Ponza, A., Berti, C., Negri, A., Sabbatini, A., 2014. Unraveling tectonic and climatic controls on synorogenic stratigraphy (Northern Apennines, Italy). GSA Bull. 126, 532 552.

Hensen, C., Nuzzo, M., Hornibrook, E., Pinheiro, L.M., Bock, B., Magalhaes, V.H., Bruckmann, W., 2007. Sources of mud volcano fluids in the Gulf of Cadiz indications for hydrothermal imprint. Geochim. Cosmochim. Acta 71 (5), 1232 1248.

Lein, A. Yu, 2004. Authigenic carbonate formation in the ocean. Lithol. Miner. Resour. 39 (1), 1 30. Translated from Litologiya i Poleznye Iskopaemye 1, 2004: 3-35.

Leoni, L., Saitta, M., 1976. X-ray fluorescence analysis of 29 trace elements in rock and mineral standards. Rend. Soc. Ital. Mineral. Petrol. 32, 497 510.
Leoni, L., Menichini, M., Saitta, M., 1982. Determination of S, Cl, and F in silicate rocks by X-Ray fluorescence analyses. X-Ray Spectrom. 11, 156 158.
Lumsden, D.N., 1979. Discrepancy between thin-section and X-ray estimates of dolomite in limestone. J. Sediment. Res. 49, 429 435.
Magalhaes, V.H., 2006 2007. Carbonates autigénicos e estruturas de escape de fluidos no Golfo de Cádis. Unpubl. Thesis (Tese apresentada do grau de Doutor em Geocencias.) Departamento de Geocencias, Universidade de Aveiro. a.a.

Magalhaes, V.H., Pinheiro, L.M., Ivanov, M.K., Kozlova, E., Blinova, V., Kolganova, J., Vasconcelos, C., McKenzie, J.A., Bernasconi, S.M., Kopf, A.J., Díaz-del-Río, V., González, F.J., Somoza, L., 2012. Formation processes of methane-derived authigenic carbonates from the Gulf of Cadiz. Sediment. Geol. 243 244, 155 168.
Mazzini, A., Aloisi, G., Akhmanov, G.G., Parnell, J., Cronin, B.T., Murphy, P., 2005. Integrated petrographic and geochemical record of hydrocarbon seepage on the Vøring Plateau. J. Geol. Soc. Lond. 162, 815 827.
Naudts, L., Greinert, J., Artemov, Y., Beaubien, S.E., Borowski, C., Batist, M.D., 2008. Anomalous sea-floor backscatter patterns in methane venting areas, Dnepr paleo-delta, NW Black Sea. Mar. Geol. 251, 253 267.
Nyman, S.L., Nelson, C.S., Campbell, K.A., 2010. Miocene tubular concretions in East Coast Basin, New Zealand: analogue for the subsurface plumbing of cold seeps. Mar. Geol. 272, 319 336.
Oppo, D., Capozzi, R., Picotti, V., 2013. A new model of the petroleum system in the Northern Apennines, Italy. Mar. Pet. Geol. 48, 57 76.
Oppo, D., Capozzi, R., Picotti, V., Ponza, A., 2015. A genetic model of hydrocarbon-derived carbonate chimneys in shelfal fine grained sediments: the Enza River field, Northern Apennines (Italy). In: Capozzi, R., Negri, A., Reithner, J., Taviani, M. (Eds.), Carbonate Conduits Linked to Hydrocarbon-enriched Fluid Escape. Special Issue of Marine and Petroleum Geology.
Orpin, A.R., 1997. Dolomite chimneys as possible evidence of coastal fluid expulsion, uppermost Otago continental slope, southern New Zealand. Mar. Geol. 138, 51 67.
Peckmann, J., Reimer, A., Luth, U., Luth, C., Hansen, B.T., Heinicke, C., Hoefs, J., Reitner, J., 2001. Methane-derived carbonates and authigenic pyrite from the northwestern Black Sea. Mar. Geol. 177, 129 150.
Peckmann, J., Thiel, V., 2004. Carbon cycling at ancient methane-seeps. Chem. Geol. 205, 443 467.
Peckmann, J., Campbell, K.A., Walliser, O.H., Reitner, J., 2007. A Late Devonian hydrocarbon-seep deposit dominated by dimerreloid brachiopods, Morocco. Palaios 22, 114 122.
Picotti, V., Capozzi, R., Bertozzi, G., Mosca, F., Sitta, A., Tornaghi, M., 2007. The Miocene petroleum system of the Northern Apennines in the central Po Plain (Italy). In: Lacombe, O., Lavé, J., Roure, F., Vergés, J. (Eds.), Thrust Belts and Foreland Basins, from Fold Kinematics to Hydrocarbon System. Springer Verlag, Berlin, pp. 117 131.
Pinheiro, L.M., Ivanov, M.K., Sautkin, A., Akhmanov, G., Magalhaes, V.H., Volkonskaya, A., Cunha, M.R., 2003. Mud volcanism in the Gulf of Cadiz: results from the TTR-10 cruise. Mar. Geol. 195, 131 151.
Ponza, A., Pazzaglia, F.J., Picotti, V., 2010. Thrust-fold activity at the mountain front of the Northern Apennines (Italy) from quantitative landscape analysis. Geo-morphology 123, 211 223.
Reitner, J., Peckmann, J., Reimer, A., Schumann, G., Thiel, V., 2005. Methane-derived carbonate build-ups and associated microbial communities at cold seeps on the lower Crimean shelf (Black Sea). Facies 51, 66 79.
Rodriguez, N.M., Paull, C.K., Borowski, W.S., 2000. Zonation of authigenic carbonates within gas hydrate-bearing sedimentary sections on the Blake Ridge: offshore southeastern North America. Proc. ODP Sci. Results 164, 301 312.
Rosenbaum, J., Sheppard, S.M.F., 1986. An isotopic study of siderites, dolomites and ankerites at high-temperatures. Geochim. Cosmochim. Acta 50 (6), 1147 1150.
Rosenbaum, J.M., 1994. Stable-isotope fractionation between carbon-dioxide and calcite at 900 °C. Geochim. Cosmochim. Acta 58 (17), 3747 3753.
Somoza, L., Díaz-del-Rio, V., Léon, R., Ivanov, M.K., Fernández-Puga, M.C., Lobato, A., Maestro, A., Hernández-Molina, F.J., Gardner, J.M., Rodero, J., Pinheiro, L.M., Vásquez, J.T., Medialdea, T., Fernández-Salas, L.M., 2003. Seabed morphology and hydrocarbon seepage in the Gulf of Cadiz mud volcano area: imagery of multibeam data and ultra-high resolution data. Mar. Geol. 195, 153 176.
Taviani, M., 2001. Fluid venting and associated processes. In: Vai, G.B., Maltini, I.P. (Eds.), Anatomy of an Orogen: the Apennines and Adjacent Mediterranean Basins. Kluwer Academic Publisher, Great Britain, pp. 351 366.
Taviani, M., 2014. Marine chemosynthesis in the Mediterranean Sea. In: Goffredo, S., Baader, H., Dubinsky, Z. (Eds.), The Mediterranean Sea: Its History and Present Challenges. Springer, Science + Business Media Dordrecht, pp. 69 83.
Teichert, B.M.A., Bohrmann, G., Suess, E., 2005. Chemoherms on Hydrate Ridge: unique microbially mediated carbonate build-ups growing into the water column. Palaeogeogr. Palaeoclimatol. Palaeoecol. 227, 67 85.
Unterseh, S.L., 2013, May 6. Early Recognition of Seabed and Sub-seabed Natural Hydrocarbon Seeps in Deep Offshore Angola. Offshore Technology Conference.
Vanneste, H., Kastner, M., James, R.H., Connelly, D.P., Fisher, R.E., Kelly-Gerreyn, B.A., Heeschen, K., Haeckel, M., Mills, R.A., 2012. Authigenic carbonates from the Darwin Mud Volcano, Gulf of Cadiz: a record of palaeo-seepage of hydrocarbon bearing fluids. Chem. Geol. 300 301, 24 39.
Wirsig, C., Kowsmann, R.O., Miller, D.J., de Oliveira Godoy, J.M., Mangini, A., 2012. U/Th dating and post-depositional alteration of a cold seep carbonate chimney from the Campos Basin offshore Brazil. Mar. Geol. 329 331, 24 33.
Zachos, J., Pagani, M., Sloan, L., Thomas, E., Billups, K., 2001. Trends, rhythms, and aberrations in global climate 65 Ma to present. Science 292, 686 693.